NAVAL POSTGRADUATE SCHOOL
Monterey, California

THESIS

UNIFORM FLOW PAST A RIGID SPHERE BY
THE SPECTRAL NUMERICAL METHODS

by

Zekai Akcan

March 1997

Thesis Advisor: Ashok Gopinath

DTIC QUALITY INSPECTED 3

19971113 050

REPORT DOCUMENTATION PAGE

Form Approved OMB No. 0704-0188

Public reporting burden for this collection of information is estimated to average 1 hour per response, including the time for reviewing instruction, searching existing data sources, gathering and maintaining the data needed, and completing and reviewing the collection of information. Send comments regarding this burden estimate or any other aspect of this collection of information, including suggestions for reducing this burden, to Washington Headquarters Services, Directorate for Information Operations and Reports, 1215 Jefferson Davis Highway, Suite 1204, Arlington, VA 22202-4302, and to the Office of Management and Budget, Paperwork Reduction Project (0704-0188) Washington DC 20503.

1. AGENCY USE ONLY *(Leave blank)*	2. REPORT DATE March 1997	3. REPORT TYPE AND DATES COVERED Master's Thesis

4. TITLE AND SUBTITLE UNIFORM FLOW PAST A RIGID SPHERE BY THE SPECTRAL NUMERICAL METHODS.	5. FUNDING NUMBERS
6. AUTHOR(S) Akcan, Zekai	
7. PERFORMING ORGANIZATION NAME(S) AND ADDRESS(ES) Naval Postgraduate School Monterey, CA 93943-5000	8. PERFORMING ORGANIZATION REPORT NUMBER
9. SPONSORING/MONITORING AGENCY NAME(S) AND ADDRESS(ES)	10. SPONSORING/MONITORING AGENCY REPORT NUMBER

11. SUPPLEMENTARY NOTES The views expressed in this thesis are those of the author and do not reflect the official policy or position of the Department of Defense or the U.S. Government.

12a. DISTRIBUTION/AVAILABILITY STATEMENT Approved for public release; distribution is unlimited.	12b. DISTRIBUTION CODE

13. ABSTRACT *(maximum 200 words)*

A steady, axially symmetric, incompressible flow past a rigid sphere is numerically simulated by using a numerical scheme based on spectral methods. The equations of motion have been reduced to a set of two nonlinear second order partial differential equations in terms of the vorticity, the stream function. The calculations have been carried out for Reynolds numbers, based on the sphere diameter, in the range 0.1 to 104.

The numerical results have verified that there is excellent agreement with Stokes flow theory at very low Reynolds numbers. At moderate to high Reynolds numbers, there is good agreement with available experimental data and flow visualization pictures. The Reynolds number at which separation occurs is estimated as 20. The approach to boundary-layer behavior with increasing Reynolds numbers is also verified by comparison with potential flow theory and analytical boundary-layer solution.

14. SUBJECT TERMS Translation flow about a rigid Sphere, Axially Symmetric Flow, Spectral Methods			15. NUMBER OF PAGES 63
			16. PRICE CODE

17. SECURITY CLASSIFICATION OF REPORT Unclassified	18. SECURITY CLASSIFICATION OF THIS PAGE Unclassified	19. SECURITY CLASSIFICATION OF ABSTRACT Unclassified	20. LIMITATION OF ABSTRACT UL

DTIC QUALITY INSPECTED 3

UNIFORM FLOW PAST A RIGID SPHERE BY THE SPECTRAL NUMERICAL METHODS

Zekai Akcan
Lieutenant Junior Grade, Turkish Navy
B.S., Turkish Naval Academy, 1991

Submitted in partial fulfillment of the
requirements for the degree of

MASTER OF SCIENCE IN MECHANICAL ENGINEERING

from the

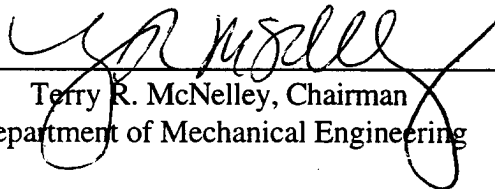## NAVAL POSTGRADUATE SCHOOL
March 1997

Author: _____
Zekai Akcan

Approved by: _____
Ashok Gopinath, Thesis Advisor

_____
Terry R. McNelley, Chairman
Department of Mechanical Engineering

ABSTRACT

A steady, axially symmetric, incompressible, viscous flow past a rigid sphere is numerically simulated by using a numerical scheme, based on spectral methods. The equations have been reduced to two sets of nonlinear second order partial differential equations in terms of vorticity and stream function. The calculations have been carried out for Reynolds numbers, based on the sphere diameter, in the range 0.1 to 104.

The numerical results have verified that there is excellent agreement with Stokes theory at very low Reynolds numbers. At moderate to intermediate Reynolds numbers there is good general agreement with available experimental data and flow visualization pictures. The Reynolds number at which separation occurs is estimated as 20. The approach to boundary-layer behavior with increasing Reynolds numbers is also verified by comparison with potential flow theory and analytical boundary-layer solution.

TABLE OF CONTENTS

I. INTRODUCTION

Numerical simulations in fluid dynamics have historically attracted considerable attention, through the use of various numerical schemes such as finite-difference and finite-element methods. In this study, the direct numerical simulation of a time-dependent, axially symmetric, incompressible viscous flow past a rigid sphere was studied by using a different numerical scheme based on spectral methods. Spectral methods have become increasingly popular in recent years, especially with the development of fast transform methods. It has been successfully applied to numerical weather predictions, numerical simulation of laminar/turbulent flows and other fundamental problems especially where high accuracy is desired for relatively lower memory requirements.

The drag dependence on Reynolds number was studied and the results were compared with the previous results. The stream function ψ and the vorticity ω were visualized through the use of the numerical results and compared with the flow visualization pictures for various Reynolds numbers. The boundary-layer thickness on the surface of the sphere was also investigated through the use of the results of the simulation. The boundary-layer thickness on the surface of the sphere is calculated by introducing the power series expansions of the stream function into the boundary-layer equations. The results are valid for $Re \rightarrow \infty$ analytically. The minimum Reynolds number for which the boundary-layer assumption is valid, is investigated by comparing the boundary-layer thickness which is obtained from the numerical solution, with analytical results in the boundary-layer limit

It is clear from the foregoing that the objective of this study is to carry out the numerical scheme based on the spectral methods, through the use of the vorticity-stream function form of the Navier-Stokes equations, on a time-dependent, axisymmetric, viscous flow about a rigid sphere. A Matlab program was developed to implement the foregoing numerical scheme. The results were compared to the previous studies which were based on different methods. However the details of the method itself were not compared to the

1

other methods which were used in previous studies. The expectations are that the results will match with the previous results, improve our current ability to compute/predict the evolution of flow for a particular geometry and conditions, and, hopefully shed some light on the physics of flows which have been heretofore uncalculated.

II. BACKGROUND STUDIES

The collocation method appears to have been first used by Slater (1934) and Kantorovic (1934) in specific applications. It was developed as a general method for solving ordinary differential equations. In 1938 Lanczos' work showed for the first time that a proper choice of trial functions and distribution of collocation points is crucial to the accuracy of solution. This method was revived by Clenshaw (1957), Norton (1963) and Wright (1964). The application of Chebyshev polynomial expansions to the initial value problems are involved in these studies.

The spectral collocation method was applied to partial differential equations for spatially periodic problems by Kreiss and Oliger (1972) (who called it the Fourier method) and Orszag (1972) (who termed it pseudospectral). These were the earliest applications of spectral collocation or pseudospectral method. This approach was very attractive because of its application to variable-coefficient and even non-linear problems.

The Galerkin approach which depends on the same trial and test functions, was applied to a meteorological model by Silberman (1954). This was the first serious application of spectral methods to PDE's. After Orszag (1969,1970) and Eliasen, Machenhauer and Rasmussen (1970) developed transform methods for evaluating convolution sums arising from quadratic non-linearity, spectral Galerkin methods only became practical for high resolution calculations of such non-linear problems.

The first unifying mathematical assessment of the theory of spectral methods was covered in the monograph by Gottlieb and Orszag (1977). Since then, the theory has been extended to cover many different problems, such as variable-coefficient and non-linear problems. Applications in fluid dynamics were reviewed in the symposium proceedings edited by Voigt, Gottlieb and Hussaini (1984). Other introductory or review articles have appeared recently such as Mercier (1981), Hussaini, Salas and Zang (1985), Zang and Hussaini (1985), Deville (1984), Gottlieb (1985) and Hussaini and Zang (1987).

It is well known that the background of this particular problem of flow over a sphere has a long history due to the fundamental interest in external flow over bluff bodies. The first theoretical results for steady, uniform flow past a rigid sphere were given by Proudman and Pearson (1957) and are valid for $Re < 1$. For higher Reynolds numbers computations have been conducted by Rimon and Cheng (1969), Le Clair, Hamielec and Pruppacher (1970) and more recently by Fornberg (1988). All these computations are based on finite-difference schemes. Dennis and Walker (1971), Oliver and Chung (1985) and Brabston and Keller (1975) used a different computational approach based on an expansion of Legendre functions and spherical harmonics. The results of these simulations are consistent with the experimental data for the drag forces, and have been used to develop improved formulae. Marcus and Tuckerman (1987) developed another technique based on the spectral methods and successfully applied it to the simulation of a flow between concentric rotating spheres. And more recently Chang and Maxey (1994) have used the same method to compute the oscillatory flow about a sphere.

III. GOVERNING EQUATIONS

A. DERIVATION OF THE EQUATIONS

The well known Navier-Stokes equations of motion of a viscous, incompressible fluid are;

$$\frac{\partial \mathbf{u}}{\partial t} + (\mathbf{u} \cdot \nabla)\mathbf{u} = -\frac{1}{\rho}\nabla p + \nu \nabla^2 \mathbf{u} \tag{3.1}$$

$$\nabla \cdot \mathbf{u} = 0 \tag{3.2}$$

Define dimensionless variables

$$r^* = \frac{r}{a} \qquad \mathbf{u}^* = \frac{\mathbf{u}}{U} \qquad \nabla p^* = \frac{\nabla p}{\rho U^2} \qquad \nabla^* = \frac{1}{a}\nabla$$

where   a: radius of the sphere

   U: free stream velocity

   ρ : density of the fluid

   ν : kinematic viscosity of the fluid

Introduce the dimensionless variables in Eq. (3.1)

$$\frac{U\nu}{a^2}\frac{\partial \mathbf{u}^*}{\partial t} + \frac{U^2}{a}(\mathbf{u}^* \cdot \nabla)\mathbf{u}^* = -\frac{1}{\rho}\frac{U^2}{a}\nabla p^* + \nu\frac{U}{a^2}\nabla^2 \mathbf{u}^* \tag{3.3}$$

Divide Eq. (3.3) by $\dfrac{U \cdot \nu}{a^2}$

$$\frac{\partial \mathbf{u}^*}{\partial t} + \frac{U \cdot a}{\nu}(\mathbf{u}^* \cdot \nabla)\mathbf{u}^* = -\frac{U \cdot a}{\nu}\nabla p^* + \nu\nabla^2 \mathbf{u}^* \tag{3.4}$$

Hereafter the superscript * will be omitted for nondimensional terms. Define the Reynolds number based on the diameter, $Re_d = \dfrac{U(2a)}{\nu}$, and take the curl of Eq. (3.4) to be able to eliminate the pressure term and introduce vorticity, $\omega = \nabla \times \mathbf{u}$ where the vorticity vector, ω, is

5

$$\omega = i_r \omega_r + i_\theta \omega_\theta + i_\Phi \omega_\Phi.$$

Because of the absence of any azimuthal fluid motion about the axis of symmetry only the Φ-component of the vorticity survives and the transport equation for the Φ-component of the vorticity is

$$\frac{\partial}{\partial t}\omega_\Phi - \left[\nabla \times (u \times \omega_\phi i_\phi)\right] \cdot i_\phi = \frac{2}{Re_d}\left(\nabla^2 - \frac{1}{r^2 \sin^2\theta}\right)\omega_\Phi \qquad (3.5)$$

Convert the velocity in Eq. (3.5) by defining the axisymmetric Stream function (ψ)

$$u = \nabla \times \left[\frac{\psi}{r \sin\theta}i_\phi\right] \qquad \phi \; ; \text{ Azimuthal direction} \qquad (3.6)$$

In spherical coordinates, Eq. (3.6) is obtained as

$$u = \left[\frac{1}{r^2 \sin\theta}\frac{\partial\psi}{\partial\theta}\right]i_r - \left[\frac{1}{r \sin\theta}\frac{\partial\psi}{\partial r}\right]i_\theta \qquad (3.7)$$

where

$$u = u_r i_r + u_\theta i_\theta + u_\Phi i_\Phi \qquad (3.8)$$

As noted earlier $u_\phi = 0$ in this study.

In the free stream $\psi = \frac{1}{2}Ur^2 \sin^2\theta$ or $\psi = \frac{1}{2}r^2 \sin^2\theta$ in nondimensional form.

By using the definition of the stream function it can be shown that

$$\omega_\Phi = \left[\frac{\partial^2\psi}{\partial r^2} + \frac{1}{r^2}\frac{1}{\sin\theta}\frac{\partial}{\partial\theta}\left(\frac{1}{\sin\theta}\frac{\partial\psi}{\partial\theta}\right)\right]\left(\frac{-1}{r\sin\theta}\right) \qquad (3.9)$$

Define an operator $\overline{D}^2$ as

$$\overline{D}^2 = \frac{\partial^2}{\partial r^2} + \frac{\sin\theta}{r^2}\frac{\partial}{\partial\theta}\left(\frac{1}{\sin\theta}\frac{\partial}{\partial\theta}\right) \qquad (3.10)$$

6

to obtain the azimuthal component of the vorticity;

$$\omega_\phi = -\frac{1}{r\sin\theta}\overline{D}^2\psi \qquad (3.11)$$

Call $[\nabla\times(\mathbf{u}\times\omega_\phi i_\phi)].i_\phi$ in Eq. (3.5) the nonlinear term $G(r,\theta,t)$.

By carrying out the calculations in spherical coordinates it can be shown that

$$\nabla\times(\mathbf{u}\times\omega_\phi i_\phi) = \frac{1}{r^3\sin\theta}\left[\frac{\partial(\psi,\overline{D}^2\psi)}{\partial(r,\mu)} + 2\overline{D}^2\psi L(\psi)\right] \qquad (3.12)$$

where

$$\mu = \cos\theta$$

$$L = \frac{\mu}{1-\mu^2}\frac{\partial}{\partial r} + \frac{1}{r}\frac{\partial}{\partial\mu} \qquad (3.13)$$

$$\frac{\partial(z_1,z_2)}{\partial(x,y)} = \frac{\partial z_1}{\partial x}\frac{\partial z_2}{\partial y} - \frac{\partial z_1}{\partial y}\frac{\partial z_2}{\partial x}$$

Combine all terms to get

$$\frac{\partial}{\partial t}(\overline{D}^2\psi) + \frac{Re_d}{2}\frac{1}{r^2}\left[\frac{\partial(\psi,\overline{D}^2\psi)}{\partial(r,\mu)} + 2\overline{D}^2\psi L(\psi)\right] = \overline{D}^4\psi \qquad (3.14)$$

Equation (3.14) is called the Vorticity-Stream function form of the Momentum equation in axisymmetric spherical coordinate system. For computational purposes, which will become clear later, define a modified stream function $C(r,\theta,t)$, which is related to the usual Stokes stream function (ψ) by the relation;

$$\psi = rC\sin\theta \qquad (3.15)$$

Also for any function $f(r,\theta)$, define a new operator D^2 such that

$$\overline{D}^2(fr\sin\theta) = r\sin\theta D^2 f$$

where

7

$$D^2 = \nabla^2 - \frac{1}{r^2 \sin^2 \theta}.$$

This gives

$$\omega_\phi = -D^2 C \qquad (3.16)$$

$$u = \nabla \times (Ci_\phi) \qquad (3.17)$$

where

$$u_r = \frac{1}{r \sin \theta} \frac{\partial}{\partial \theta} (C \sin \theta)$$

$$u_\theta = -\frac{1}{r} \frac{\partial}{\partial r} (rC) \qquad (3.18)$$

The modified stream function C is written as the sum $C = \overline{C} + c$, where $\overline{C} = \frac{1}{2} r \sin \theta$, (which is the prescribed uniform-flow free stream condition), and c represents the disturbance produced by the presence of the rigid sphere.

Returning to Eq. (3.5), rearrange by multiplying both sides with $r^2 \dfrac{Re_d}{2}$,

$$r^2 \frac{Re_d}{2} \frac{\partial \omega}{\partial t} = r^2 \frac{Re_d}{2} G(r, \theta, t) + r^2 D^2 \omega \qquad (3.19)$$

$$r^2 D^2 C = -r^2 \omega \qquad (3.20)$$

where the nonlinear term

$$G(r, \theta, t) = \left[\nabla \times (u \times \omega_\phi i_\phi) \right] \cdot i_\phi \qquad (3.21)$$

and the operator D^2 is defined as

$$D^2 = \frac{1}{r^2} \frac{\partial}{\partial r} \left(r^2 \frac{\partial}{\partial r} \right) + \frac{1}{r^2 \sin^2 \theta} \frac{\partial}{\partial \theta} \left(\sin \theta \frac{\partial}{\partial \theta} \right) - \frac{1}{r^2 \sin^2 \theta} \qquad (3.22)$$

8

B. BOUNDARY CONDITIONS

The flow is determined by numerically solving (3.5) for the vorticity and (3.20) for the modified stream function C subject to the boundary conditions;

$$\mathbf{u} = 0 \qquad\qquad\qquad \text{at } r = 1 \qquad\qquad (3.23)$$

$$\mathbf{u} = U(t) \text{ "free stream velocity"} \quad \text{as } r \to \infty \qquad (3.24)$$

Boundary conditions (3.23) and (3.24) may be reformulated in terms of C as

$$C = 0, \quad \frac{\partial C}{\partial r} = 0 \qquad \text{on } r = 1 \qquad\qquad (3.25)$$

$$\omega = 0, \quad C = \frac{1}{2} U(t) r \sin(\theta) \qquad \text{as } r \to \infty \qquad (3.26)$$

The Neumann Boundary Conditions in Equation (3.25) are handled with the Green's function method that will be explained later. Homogenous boundary conditions on the axis of symmetry ($\theta = 0, \pi$) are automatically satisfied with the choice of the sine series expansions in the numerical method as shown later.

C. BOUNDARY LAYER BEHAVIOR

The boundary layer thickness on the surface of the sphere can be calculated with the method of power series expansion as discussed in, Schlichting (1987,pp.235-238). The body contour of the sphere with radius a is defined by $r(x) = a \sin(x / a)$ where x is the distance along the surface from the stagnation point. In the boundary-layer limit the velocity distribution near the surface of the sphere is given by $U(x) = \frac{3}{2} U_\infty \sin(x / a)$.

By introducing the stream-function into the boundary-layer equations the final form of the transformation is obtained for axially symmetrical case;

9

$$\frac{\partial \psi}{\partial y}\frac{\partial^2 \psi}{\partial x \partial y} - \left(\frac{\partial \psi}{\partial x} + \frac{1}{r}\frac{dr}{dx}\psi\right)\frac{\partial^2 \psi}{\partial y^2} = U\frac{dU}{dx} + v\frac{\partial^3 \psi}{\partial y^3} \qquad (3.27)$$

with the boundary conditions

$$y = 0 \qquad \psi = 0 \ , \quad \frac{\partial \psi}{\partial y} = 0 \qquad\qquad (3.28a)$$

$$y = \infty \qquad \frac{\partial \psi}{\partial y} = U(x) \qquad\qquad (3.28b)$$

The potential flow is defined by the series expansion as

$$U(x) = u_1 x + u_3 x^3 + u_5 x^5 + ... \qquad (3.29)$$

where $\quad u_1 = \dfrac{3}{2}\dfrac{U_\infty}{a} \ ; \quad u_3 = -\dfrac{1}{4}\dfrac{U_\infty}{a^3} \ ; .... \quad \eta = \dfrac{y}{a}\sqrt{\dfrac{3U_\infty a}{v}}$

and the body contour is expanded to series with the same way;

$$r(x) = r_1 x + r_3 x^3 + r_5 x^5 + ... \qquad (3.30)$$

The stream-function is represented by the Blasius series in analogy with (3.29) & (3.30) as;

$$\psi(x,y) = \sqrt{\frac{v}{2u_1}}\left\{u_1 x f_1(\eta) + 2u_3 x^3 f_3(\eta) + ...\right\} \qquad (3.31)$$

By introducing equations (3.29),(3.30) and (3.31) into equation (3.27) we obtain a set of differential equations for the functions $f_1, f_3, ...$

If the first two terms of the expanded series are concerned the first equation is

$$f_1''' = -f_1 f_1'' + \frac{1}{2}(f_1'^2 - 1) \qquad (3.32)$$

where differentiation with respect to η is denoted by primes. The boundary conditions are;

$$\eta = 0 \qquad f_1 = f_1' = 0 \qquad\qquad (3.33a)$$

$$\eta = \infty \qquad f_1' = 1 \qquad\qquad (3.33b)$$

10

and the second equation is

$$f_3''' = 2f_1' f_3' - 2f_1'' f_3 - \frac{1}{2} f_1 f_1'' - f_1 f_3'' - 1 \qquad (3.34)$$

with boundary conditions

$$\eta = 0 \qquad f_3 = f_3' = 0 \qquad (3.35a)$$

$$\eta = \infty \qquad f_3' = \frac{1}{2} \qquad (3.35b)$$

After solving the Eq. (3.32) and Eq. (3.34) for f_1 and f_3 the stream function and the velocity can be calculated by using Eq. (3.31). In the boundary layer limit the boundary-layer thickness (at a given angular location) is chosen to be the radial distance from the surface of the sphere where the velocity reaches to its peak value. By using the definition of η it can be shown that

$$\eta_{peak} = (r_{peak} - 1) \sqrt{\frac{3}{2} Re_d} \qquad (3.36)$$

where r_{peak} is the nondimensional distance where the velocity reaches its peak value.

By using Eq. (3.36) the calculated η_{peak} values through the use of foregoing explanations are compared with the corresponding r_{peak} values which are obtained from the numerical results. The η_{peak} values are valid as $Re_d \rightarrow \infty$ and they are compared with the boundary-layer thickness obtained from the numerical results.

IV. NUMERICAL REPRESENTATION

A. COMPUTATIONAL METHOD

A numerical scheme called the pseudospectral or collocation method based on a recent paper by Chang & Maxey(1994) which is in term based on a technique developed by Marcus & Tuckerman (1987) is used to solve the Navier-Stokes equations. Spectral methods involve representing the solution to a problem as truncated series of known functions. From this point of view, spectral methods may be viewed as extreme development of the method of weighted residuals (MWR). The trial and the test functions are the key elements of the MWR. This is also true for the spectral methods. The key difference lies in the choice of the trial and test functions. The trial functions (also called the expansion or approximating functions) and the test functions (also known as weight functions) are chosen as infinitely differentiable global functions in spectral methods. Functions are transformed between physical space and spectral space through the use of Fast Fourier Transform (FFT) and Inverse Fast Fourier Transform (IFFT) which are numerically cheap and quick to compute. Although they are not exact due to aliasing and truncating errors they rapidly converges and few frequency modes are required to obtain accurate results.

A physical process can be described either in time domain, by the values of same h as a function of t, e.g., h(t), or else in frequency domain, where the process is specified by giving its amplitude H, as a function of frequency f, that is H(f), with $-\infty < f < \infty$. If h(t) is real and even then H(f) is real and even or if h(t) is real and odd then H(f) is imaginary and odd. The processes can be transformed to either spectral domain or physical domain by using the Fourier transform equations. As it will be explained later in this chapter, we are dealing with odd functions by using sine series expansions for ω, c. The properties of odd and even functions are also valid for their derivatives and these properties will help to increase the computational efficiency in the calculations.

The functions which are introduced into the governing equations are presented both in spectral space as a finite series of trial functions and by values at collocation grid points in physical space. The vorticity ω and the modified stream function C are expanded as a Chebyshev polynomial in the radial direction and as sine series in the azimuthal direction. The calculations in the radial direction are done in physical space while the derivatives in azimuthal direction are obtained in spectral space. Since each sine term in the expansion satisfies the homogenous θ boundary conditions ($\omega = 0$, $\Psi = 0$ at $\theta = 0,\pi$) exactly, no further θ boundary conditions need to be applied.

In general let a variable, say ω, be expressed as

$$\omega(r,\theta,t) = \sum_{n=1}^{N} \omega_n(z,t)\mathrm{Sin}\theta_n \qquad (4.1a)$$

with

$$\omega_n(z,t) = \sum_{m=0}^{M} \omega_{mn}(t)T_m(z) \qquad (4.1b)$$

where $T_m(z)$ is Chebyshev Polynomial with $-1 \leq z \leq 1$

$$\theta_n = \frac{n\pi}{N+1} \qquad n = 1,2,...N \qquad (4.2)$$

$$z = \mathrm{Cos}\left(\frac{m\pi}{M}\right) \qquad m = 0,1,...M \qquad (4.3)$$

An algebraic map is used to map the radial interval $1 \leq r \leq r_\infty$ to the interval $-1 \leq z \leq 1$ where

$$r = \left(1 + L\frac{1+z}{b-z}\right)^{\frac{1}{\alpha}} \qquad |z| \leq 1 \qquad (4.4)$$

with $\qquad b = 1 + \dfrac{2L}{r_\infty^\alpha - r_o}$ (note that $r_o = 1$, the surface of the sphere)

L is a scaling parameter which is used to map the radial interval to the z-interval. A finite, but large outer r_∞ was chosen to avoid regularity problems in the radial differentiation. Another mapping parameter,α is defined for higher Reynolds numbers

($Re_d \geq 20$). For small Reynolds numbers α is taken as 1. Two typical grids for two different parameters are shown in Figure 1.
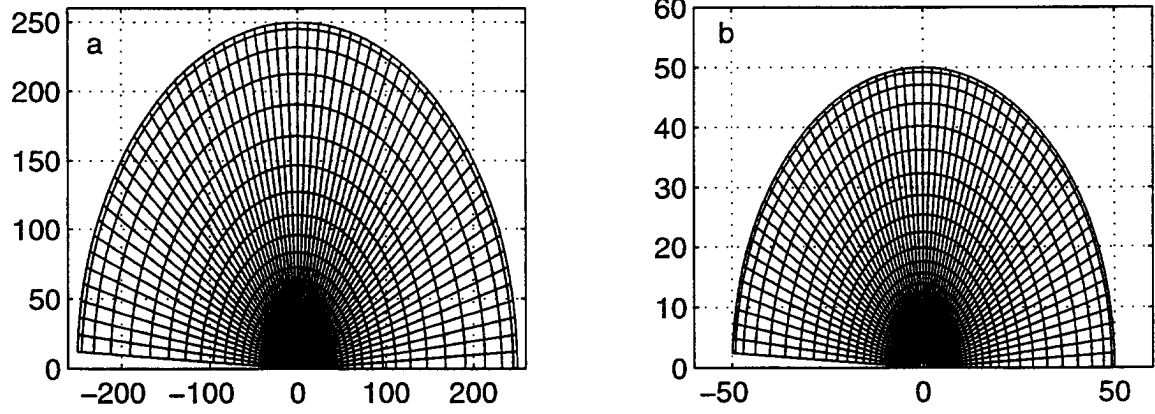

Figure 1. Typical grids for α=1 a)L=8 rinf=250 M=64 N=64 b) L=2 rinf=50 M=64 N=64

The sine expansions in Eq.(4.1a) and Eq.(4.1b) for ω and C satisfy the homogenous θ boundary conditions and match exactly the periodicity and symmetry conditions in θ. The solution of the elliptic Eq.(3.20) is required to obtain the modified stream function C from vorticity ω at any time level. Following Marcus & Tuckerman (1987) separable derivative operators D_r^2 and D_θ^2 are defined as

$$r^2 D^2 = D_r^2 + \frac{1}{\sin^2 \theta} D_\theta^2 \qquad (4.5)$$

where

$$D_r^2 = \frac{\partial}{\partial r}\left(r^2 \frac{\partial}{\partial r}\right)$$

$$D_\theta^2 = \left[\sin\theta \frac{\partial}{\partial\theta}\left(\sin\theta\frac{\partial}{\partial\theta}\right) - 1\right] \qquad (4.6)$$

In spectral θ-space the effect of operator D_θ^2 at any fixed radial location (physical r-space) can be written as

$$D_\theta^2 . f(\theta) = \left[\sin^2\theta\frac{\partial^2}{\partial\theta^2} + \sin\theta\cos\theta\frac{\partial}{\partial\theta} - 1\right]\sum f_j \sin(j\theta)$$

$$... = \sum_{j=1}^{N} f_j \left[-(1 + \frac{1}{2}j^2)\sin(j\theta) + \frac{1}{4}j(1 + j)\sin(2\theta + j\theta) + \frac{1}{4}j(1 - j)\sin(2\theta - j\theta)\right] \qquad (4.7)$$

15

If we write this expression in the form of $D_\theta^2 f(\theta) = [S_{ij}] f_j$ we get

$$S_{ij} = \begin{cases} \dfrac{(i-2)(i-1)}{4} \dots\dots\dots i = j+2 \\[2mm] -1 - \dfrac{i^2}{2} \dots\dots\dots\dots i = j \\[2mm] \dfrac{(i+2)(i+1)}{4} \dots\dots\dots i = j-2 \\[2mm] 0 \dots\dots\dots\dots\dots\dots\text{otherwise} \end{cases} \qquad (4.8)$$

This matrix is NxN if the representation for $D_\theta^2 f$ is truncated to N Fourier terms. Similarly the operation of multiplying a function $f(\theta)$ by $\sin^{-2}\theta$ produces another NxN matrix which is called A matrix where the only non-zero terms are ;

$$A_{ij} = \begin{cases} a1(i) = -i(i+1) \dots\dots\dots i = j \\[2mm] a2(i) = -2i \dots\dots\dots\dots i < j, i+j = \text{even} \end{cases} \qquad (4.9)$$

B.   TIME INTEGRATION

Time integration of the Eq.(3.19) and Eq.(3.20) are accomplished through the use of an explicit second-order Adams-Bashforth scheme for the nonlinear terms and an implicit second-order Crank-Nicholson scheme for the viscous and linear terms. The calculations are made in physical r-space and spectral θ-space. If we denote vorticity $\omega(r,t)$ as the vector of N sine series then discretized forms of Eq.(3.19) and Eq.(3.20) are;

$$r^2 \frac{Re_d}{2} \left[\frac{\omega_{t+\Delta t} - \omega_t}{\Delta t} \right] = r^2 \frac{Re_d}{2} \left[\alpha G_t + \beta G_{t-\Delta t} \right] + \left[D_r^2 + A \right] \left(\frac{\omega_t + \omega_{t+\Delta t}}{2} \right) \qquad (4.10)$$

Rearrange Eq.(4.10) and get ;

$$\left[D_r^2 + A - r^2 \frac{Re_d}{\Delta t} \right] \omega_{t+\Delta t} = - \left[D_r^2 + A + r^2 \frac{Re_d}{\Delta t} \right] \omega_t - r^2 Re_d \left[\alpha G_t - \beta G_{t-\Delta t} \right] \qquad (4.11)$$

where $\alpha = \dfrac{3}{2}; \beta = -\dfrac{1}{2}$ and $G(r,\theta,t) = [\nabla \times (u \times \omega)] i_\phi$

Equation (3.20) is also discretized by using the same method as ;

16

$$\left[D_r^2 + A\right]c(r, t + \Delta t) = -r^2\omega(r, t + \Delta t) \tag{4.12}$$

The radial derivatives are evaluated by collocation methods and expressed as matrix operations on the vector of function values at the grid points in physical r-space. For (M+1) collocation points, we introduce the (M+1)x (M+1) matrix operation, that is

$$D^{(1)}(n) = D_r^2 + \left[a(1) - \frac{Re_d}{\Delta t}r^2\right]I \tag{4.13}$$

where, I is the identity matrix. The operator $[D_r^2 - r^2(Re_d/\Delta t) + A]$ in Eq.(4.11) may now be written in block matrix form as

$$\begin{bmatrix}
D^{(1)}(1) & 0 & a2(1)I & 0 & \cdots \\
0 & D^{(1)}(2) & 0 & a2(2)I & \cdots \\
0 & 0 & D^{(1)}(3) & 0 & \cdots \\
0 & 0 & 0 & D^{(1)}(4) & \cdots \\
\cdots & \cdots & \cdots & \cdots & \cdots
\end{bmatrix} \tag{4.14}$$

This matrix acts on the vector of a length of (M+1) x N for vorticity coefficients. Eq.(4.11) and Eq.(4.12) are upper triangular, block matrix problems in physical r-space and spectral θ-space that can be solved by any solver with the Dirichlet boundary conditions discussed below. The Eq.(3.32) is treated in the same manner and leads to an upper triangular, block matrix problem with each diagonal term on row n replaced by $D_r^2 + a1(n)I$.

C. NONLINEAR TERMS

If one opens the nonlinear term $G(r, \theta, t)$ in spherical coordinates gets six terms;

$$-\frac{1}{r}\frac{\partial\omega_\phi}{\partial r}\frac{\partial C}{\partial\theta} \qquad \frac{1}{r}\frac{\partial\omega_\phi}{\partial\theta}\frac{\partial C}{\partial r} \qquad -\frac{\cot(\theta)}{r}\omega_\phi\frac{\partial C}{\partial r}$$

$$\tag{4.15}$$

$$-\frac{\cot(\theta)}{r}C\frac{\partial\omega_\phi}{\partial r} \qquad \frac{\omega_\phi}{r^2}\frac{\partial C}{\partial\theta} \qquad \frac{C}{r^2}\frac{\partial\omega_\phi}{\partial\theta}$$

The nonlinear terms in Eq.(4.15) are handled by transforming the spectral coefficients to physical space first and transforming the result of the products to spectral

17

space after the multiplication. Basically the derivatives are obtained in spectral space and the products are done in physical space and finally the result is transformed to spectral space.

D.   GREEN'S FUNCTION METHOD

In order to enforce the radial boundary conditions in Eq.(4.11) and Eq.(4.12), Green's function method has been developed which gives the correct boundary conditions in Eq.(3.25) and Eq.(3.26) and allows the surface vorticity to develop naturally. If ω and c consist of two parts, homogenous and particular solutions, we write

$$\omega = \omega_p + \sum_{j=1}^{N} \lambda_j \tilde{\omega}_j \qquad \text{and} \qquad c = c_p + \sum_{j=1}^{N} \lambda_j \tilde{c}_j \qquad j = 1,2,\ldots\ldots N \qquad (4.16)$$

If we introduce Eq.(4.16) into Eq.(4.11) and Eq.(4.12), we find the homogenous parts with corresponding boundary conditions as follows;

$$E^2 \tilde{\omega}_j(r,\theta) = 0 \qquad (4.17) \quad H^2 \tilde{c}_j = -r^2 \tilde{\omega}_j \qquad (4.18)$$

$$\tilde{\omega}_j(r = 1,\theta_i) = \delta_{ij} \qquad\qquad \tilde{c}_j(r = 1,\theta_i) = 0$$

$$\tilde{\omega}_j(r = \infty,\theta_i) = 0 \qquad\qquad \tilde{c}_j(r = \infty,\theta_i) = 0$$

The particular parts with corresponding boundary conditions are ;

$$E^2 \omega_p(r,\theta,t+\Delta t) = R(r,\theta,t) \quad (4.19) \quad H^2 c_p(r,\theta,t+\Delta t) = -r^2 \omega_p(r,\theta,t) \qquad (4.20)$$

$$\omega_p(r = 1,\theta) = 0 \qquad\qquad c_p(r = 1,\theta) = -\overline{Cl}_{r=1}$$

$$\omega_p(r = \infty,\theta) = 0 \qquad\qquad c_p(r = \infty,\theta) = 0$$

E^2 and H^2 are obtained from block matrix defined as in Eq.(4.14)

To find λ, we enforce $\dfrac{\partial c}{\partial r}\Big|_{r=1} = -\dfrac{\partial \overline{C}}{\partial r}\Big|_{r=1}$ \hfill (4.21)

If we substitute Eq.(4.16) into Eq.(4.21), we get

$$\frac{\partial c_p}{\partial r}\Bigg|_{r=1,\theta_i} + \sum_{j=1}^{N} \frac{\partial \tilde{c}_j}{\partial r}\Bigg|_{r=1,\theta_i} \lambda_j = -\frac{\partial \overline{c}}{\partial r}\Bigg|_{r=1,\theta_i} \qquad (4.22)$$

18

Let $\left[-\dfrac{\partial \bar{c}}{\partial r} - \dfrac{\partial c_p}{\partial r}\right]_{r=1,\theta_i} = H_i$ and $\dfrac{\partial \tilde{c}_j}{\partial r}\bigg|_{r=1,\theta_i} = A_{ij}$ (4.23)

finally from Eq.(4.21),Eq.(4.22) and Eq.(4.23), we find $H_i = \displaystyle\sum_{j=1}^{N} A_{ij}\lambda_j$ and solve for

λ_j as $\lambda = A^{-1}H$. These λ values can now be used in Eq.(4.16) to arrive at the values of ω

and c.

V. DISCUSSION OF THE RESULTS

The results are going to be discussed in three parts. The drag coefficients calculated by following the explanation below for various Reynolds numbers are compared with the results of Chang & Maxey (1994) and the streamlines contours are compared with the experimental flow visualization pictures and finally the boundary-layer behavior in the boundary-layer limit is discussed by using the numerical results.

A. EVALUATION OF THE DRAG

By integrating the contributions from the stress tensor σ_{ij} over the sphere surface the resultant fluid force on the sphere exerted by the moving fluid is found as;

$$F_i = \oint \sigma_{ij} n_j dS \qquad (5.1)$$

where n is the unit outward normal. There is no lift force because the flow is axisymmetric and the force F acts parallel to the free-stream velocity U. The components of the force can be expressed in terms of the spherical polar coordinates as ;

$$F_1 = \oint \left(\sigma_{rr} \cos(\theta) - \sigma_{r\theta} \sin(\theta) \right) dS \qquad (5.2)$$

The normal component of the stress σ_{rr} is

$$\sigma_{rr} = -p + 2\rho\nu \frac{\partial u_r}{\partial r} \qquad (5.3)$$

The no slip boundary conditions in Eq.(3.23) and the condition of incompressible flow in Eq.(3.2) causes the $\partial u_r / \partial r$ to vanish on the surface of the sphere and the only contribution from σ_{rr} is through pressure. The shear stress $\sigma_{r\theta}$ is

$$\sigma_{r\theta} = 2\rho\nu \left[\frac{r}{2} \frac{\partial}{\partial r} \left(\frac{u_\theta}{r} \right) + \frac{1}{2r} \frac{\partial u_r}{\partial \theta} \right] \qquad (5.4)$$

21

Equation (5.3) and Eq.(5.4) are in dimensional form. By using the non-dimensional variables the drag force C_d is defined as

$$C_d = F_1 / \pi \rho a^2 U_o^2 \tag{5.5}$$

The drag force C_d may be split into two separate parts, C_f for the frictional component due to shear stress and C_p for the pressure component. The frictional component is calculated from Eq.(5.2) and Eq.(5.4) as

$$C_f = -\frac{4}{Re} \int_0^\pi \omega(r = 1, \theta) \sin^2(\theta) d\theta \tag{5.6}$$

The pressure component C_p in non-dimensional form

$$C_p = -\int_0^\pi p(r = 1, \theta) \sin(2\theta) d\theta \tag{5.7}$$

The pressure variation over the surface of the sphere can be determined once the vorticity field is known :

$$p(r = 1, \theta) = p(1, \pi) - \frac{2}{Re} \int_0^\pi \frac{\partial}{\partial r}(r\omega) \Big|_{r=1} d\theta' \tag{5.8}$$

A non-dimensional pressure coefficient $k(\theta)$ can be defined to make the calculations easier;

$$k(\theta) = 2p(r = 1, \theta) \tag{5.9}$$

The pressure at the stagnation point, $\theta = \pi$, can be evaluated from the radial momentum equation as;

$$k(\pi) = 2p(r = 1, \pi) = 1 + \frac{8}{Re} \int_1^\infty \frac{1}{r} \frac{\partial \omega}{\partial \theta} \Big|_{\theta=\pi} dr \tag{5.10}$$

B.   STEADY FLOWS

In order to verify the numerical method and to provide a comparison, simulations for steady, unidirectional flow were carried out for $Re \leq 104$. The parameters which were used in the calculations are listed in Table 1.

For all calculations the flow is initially at rest and then a uniform, constant external flow is introduced in the direction of $\theta = \pi$ and the simulation continued till the solution has converged to steady state. Two different grids were used in the calculations. A spatial discretization of 64x64 grid points was used for $Re \leq 10$ and a relatively finer mesh of 128x128 grid points was used for $Re \geq 20$. For $Re \geq 20$ a mapping parameter "α" is defined for finer resolution near the surface. The vorticity diffuses over a large region at low Reynolds numbers compared to the sphere radius while it is convected downstream with a more complex structure, which needs increased resolution.

Re	L	α	M	N	Δt	r_∞
0.1	8	1	64	64	0.05	250
0.2	8	1	64	64	0.05	250
0.3	8	1	64	64	0.05	250
0.4	8	1	64	64	0.05	250
0.5	8	1	64	64	0.05	250
0.6	8	1	64	64	0.05	250
0.7	8	1	64	64	0.05	250
0.8	8	1	64	64	0.05	250
0.9	8	1	64	64	0.05	250
1.0	8	1	64	64	0.05	250
5	2	1	64	64	0.02	50
10	2	1	64	64	0.02	50
20	1.5	1.5	128	128	0.02	50
30	1.5	1.5	128	128	0.01	40
40	1.5	1.5	128	128	0.01	30
56.5	1.5	1.5	128	128	0.01	30
104	1.5	1.5	128	128	0.005	25

Table 1. Parameters used in the calculations

The present results have been summarized in Table 2 with the previous results which were calculated by Chang & Maxey (1994). As it can be seen in Table 2 there is a general agreement between the present results and the previous results. The separation angle, θ_s, and the ratio of bubble length (s) to the diameter of sphere (d) are plotted later in this chapter to compare them with the results which were obtained experimentally by Taneda (1956).

23

Re	Present Results					Chang & Maxey				
	C_f	C_p	$k(\pi)$	θ_s	s/d	C_f	C_p	$k(\pi)$	θ_s	s/d
0.1	81.36	40.8	62.28	--	--	81.8	40.8	62.3	--	--
0.2	41.14	20.82	31.94	--	--	41.5	20.7	32.1	--	--
0.3	27.8	14.05	21.94	--	--	28.1	14.0	22.0	--	--
0.4	21.1	10.84	16.87	--	--	21.3	10.7	16.9	--	--
0.5	17.16	8.71	13.89	--	--	17.3	8.63	13.9	--	--
0.6	14.44	7.35	11.86	--	--	14.6	7.28	11.9	--	--
0.7	12.51	6.4	10.4	--	--	12.6	6.32	10.4	--	--
0.8	11.13	5.64	9.3	--	--	11.2	5.6	9.29	--	--
0.9	9.91	5.13	8.41	--	--	10.0	5.03	8.43	--	--
1.0	9.07	4.67	7.77	--	--	9.12	4.57	7.74	--	--
5	2.38	--	2.59	--	--	2.41	1.26	2.61	--	--
10	1.41	--	1.86	--	--	1.43	0.784	1.87	--	--
20	0.857	--	1.46	8.02	0.044	0.863	0.538	1.46	--	--
30	0.654	--	1.316	26.93	0.138	0.658	0.427	1.32	26.82	0.136
40	0.54	--	1.244	35.35	0.272	0.542	0.374	1.25	35.2	0.267
56.5	0.426	--	1.178	41.66	0.586	--	--	--	--	--
104	0.288	--	1.10	54.89	0.915	--	--	--	--	--

Table 2. Computed friction coefficients (C_f), pressure coefficients (C_p), forward stagnation point pressure coefficients ($k(\pi)$), separation angles (θ_s) in degrees and the ratio of bubble length to the diameter (s/d) compared with the results of Chang & Maxey.

Figure 2 shows the variation of vorticity and streamlines in the vicinity of the sphere at Re = 0.1. As it can be noticed the vorticity is diffusing over a large region and very slight asymmetry about $\theta = \pi / 2$ is observable.
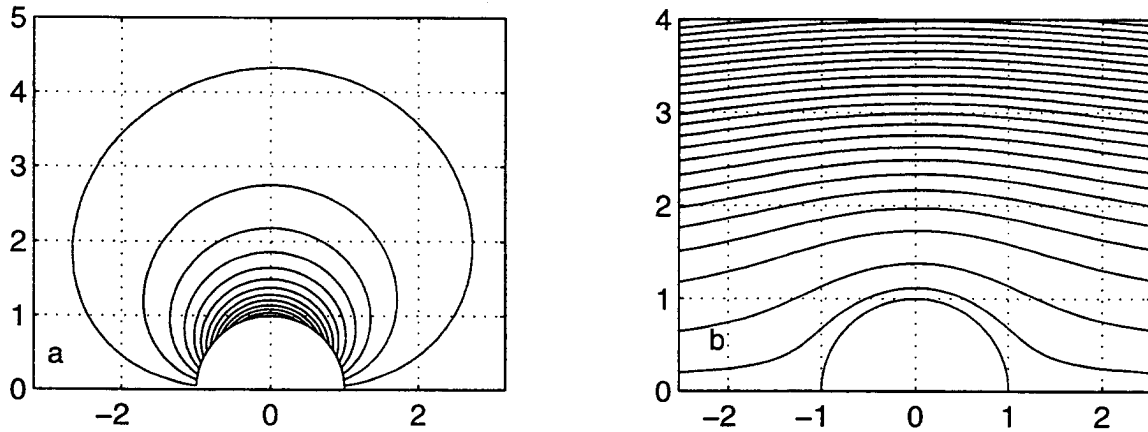

Figure 2. (a) Lines of constant vorticity for Re = 0.1 $\Delta\omega$ = 0.1 (b) Streamlines $\Delta\psi$ = 0.3

Figure 3 shows the constant vorticity and streamlines contours for Re = 5 .The asymmetric region is getting more observable about $\theta = \pi / 2$ as Reynolds number increases.
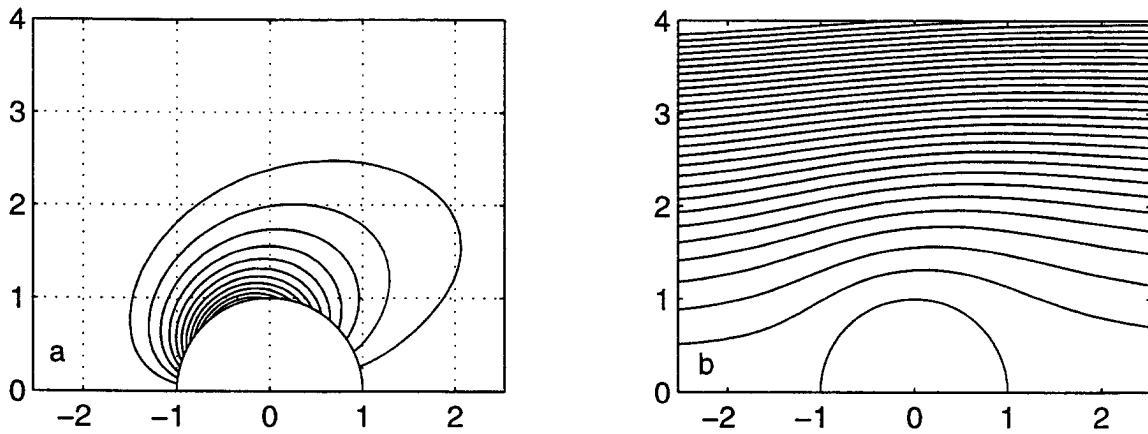

Figure 3. (a) Lines of constant vorticity for Re = 5 $\Delta\omega$ = 0.15 (b) Streamlines $\Delta\psi$ = 0.25

In Figure 4 the constant vorticity and streamlines contours are plotted for Re = 40. A separation region is clearly observable on both plots. The recirculation in the separation region is also noticeable with the asymmetry over the sphere.
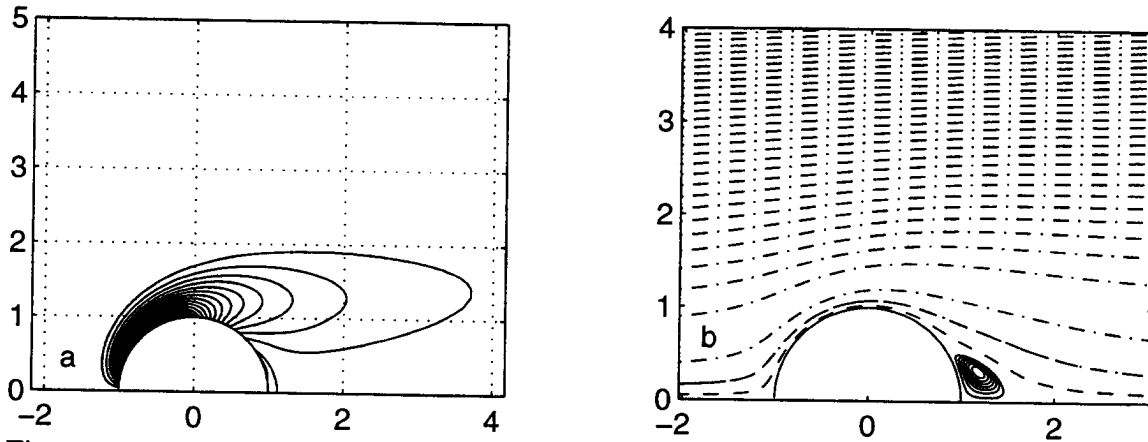
Figure 4. (a) Lines of constant vorticity for Re = 40 $\Delta\omega$ = 0.1 (b) Streamlines $\Delta\psi$ = 0.05 for '----', $\Delta\psi$ = 0.005 for '-.-.-.-', $\Delta\psi$ = 0.00004 for the separation region.

Figure 5 magnifies the separation region over the constant streamline contours for Re = 40. There is a distortion of the vorticity field caused by advection in the flow and a separation is clearly visible with a small region of negative streamlines in recirculation.
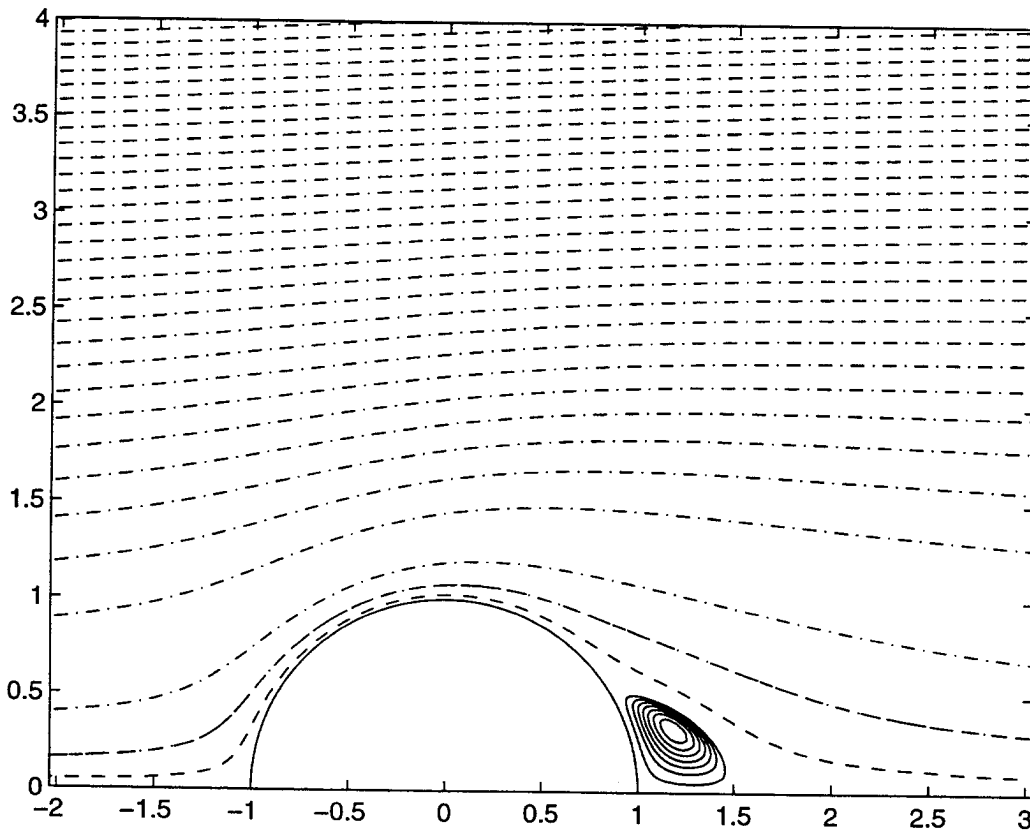

Figure 5. Constant streamline contours for Re = 40. $\Delta\psi$ = 0.00004 in the separation region , $\Delta\psi$ = 0.005 for '-.-.-.-', $\Delta\psi$ = 0.2 for '- - - - '

26

Figure 6 shows the constant vorticity and streamlines for Re = 56.5. The separation and the recirculation inside the separation region is clearly visible. There is a noticeable change in the wake length as the Reynolds number is increased from Re = 40 to Re = 56.5.
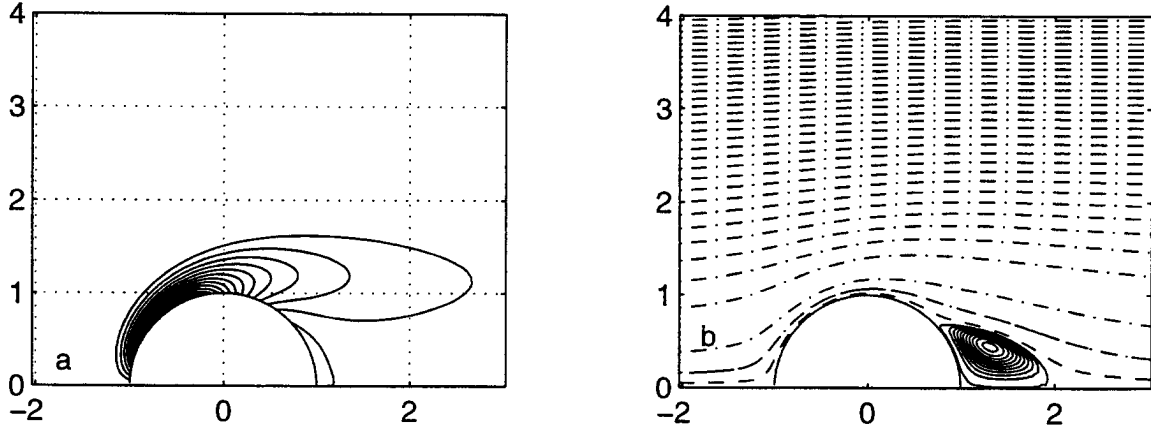

Figure 6.(a) Constant vorticity contours for Re = 56.5 Δω = 0.3 (b) Streamline contours Δψ =0.005 for '----', Δψ = 0.15 for '-.-.-.-', Δψ = 0.0003 for the separation region.

The constant vorticity and streamline contours for Re = 104 are plotted in Figure 7. The separation region and recirculation inside the separated flow is clearly visible. The increase in the wake length is also noticeable for this particular Reynolds number. It is also noticeable from the foregoing plots that the vorticity diffuses to smaller region as Reynolds number increases.
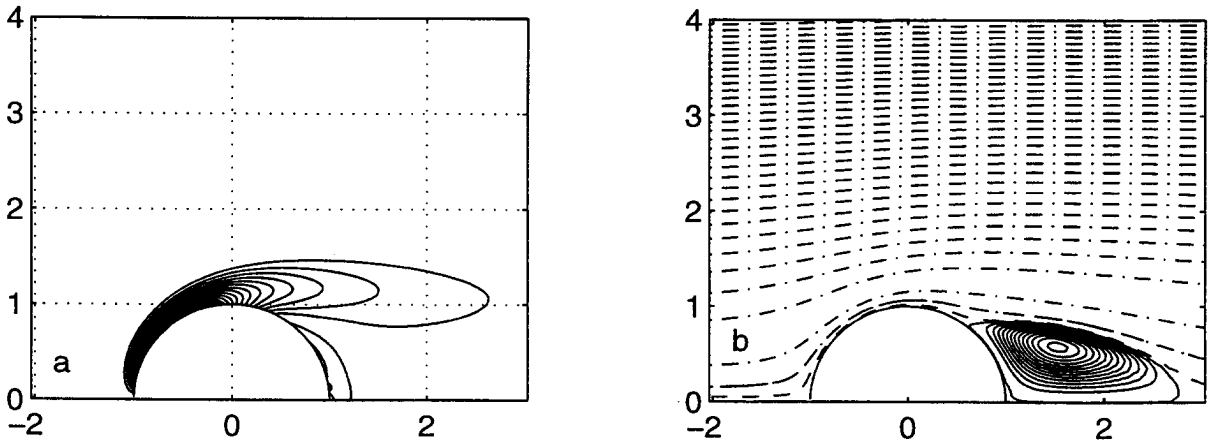

Figure 7. (a) Lines of constant vorticity for Re = 104 Δω = 0.4 (b) Streamlines Δψ =0.005 for '----', Δψ = 0.15 for '-.-.-.-', Δψ = 0.0009 for the separation region for Re = 104.

Figure 8 magnifies the streamlines for Re = 56.5. The flow visualization picture for same Reynolds number is also presented in Figure 9. It is clearly observable that there is a similarity between Figure 8 and Figure 9. The wake length, separation location and the nature of the streamlines in Figure 8 and Figure 9 look alike in both figures for the numerical results and flow visualization picture.

Figure 10 magnifies the streamlines plot for Re = 104 to present the similarity of it with the flow visualization picture in Figure 11 for the same Reynolds number. The extension of the recirculating wake to a full diameter in the downstream is clearly visible in Figure 10 and Figure 11. The flow is still laminar at this Reynolds number.

The calculated separation angles and the ratio of the wake lengths to the diameter of the sphere are presented in Figure 12 respectively along with the experimental data which were obtained by Taneda (1956). There is a good agreement between the present results and Taneda's data. Taneda has also extrapolated his data and conjectured the critical Reynolds number of the "onset of separation" as $Re_c = 24$. On the other hand, the earlier work of Nisi&Porter (1926),which was specially designed to detect the onset of separation with ultramicroscopic methods, reported separation at Re = 10 and indicated that the onset of separation in an infinite fluid is about $Re_c \cong 8$.

An estimate of Re = 20 is given by the present results as the Reynolds number for the onset of separation. This is good agreement with the value of $Re_c = 20.7$ given by Chang&Maxey (1994), the value of $Re_c = 20.5$ given by Dennis&Walker (1971) and the value of $Re_c = 20$ given by both Le Clair et al.(1970) and Lin&Lee (1973). Others have found separation to first occur at different Reynolds numbers, for example Rimon&Cheng (1969) found separation as low as $Re_c = 10$.

Taneda's data also suggests that the length of the separation bubble varies linearly with the logarithm of the Reynolds number. The present results are consistent with such a result and they remark that over this limited range a simple linear relationship with Reynolds number is a good approximation.
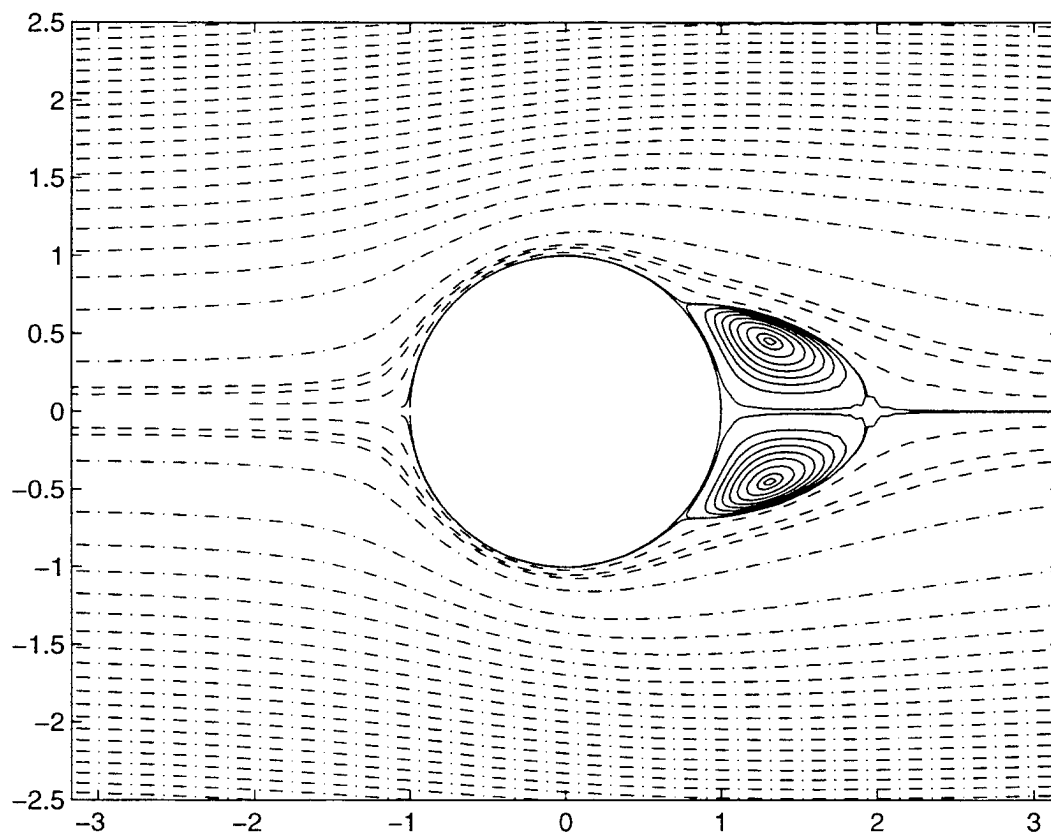
Figure 8. Streamlines $\Delta\psi = 0.005$ for '----', $\Delta\psi = 0.15$ for '-.-.-.-', $\Delta\psi = 0.0003$ for the separation region for Re = 56.5

Figure 9. The flow visualization picture of streamlines for Re = 56.5 (Archives de l'Academie des Sciences de Paris. Payard & Coutanceau 1974)

29

Figure 10. Streamlines $\Delta\psi$ =0.005 for '----', $\Delta\psi$ = 0.15 for '-.-.-.-', $\Delta\psi$ = 0.0009 for the separation region for Re = 104.
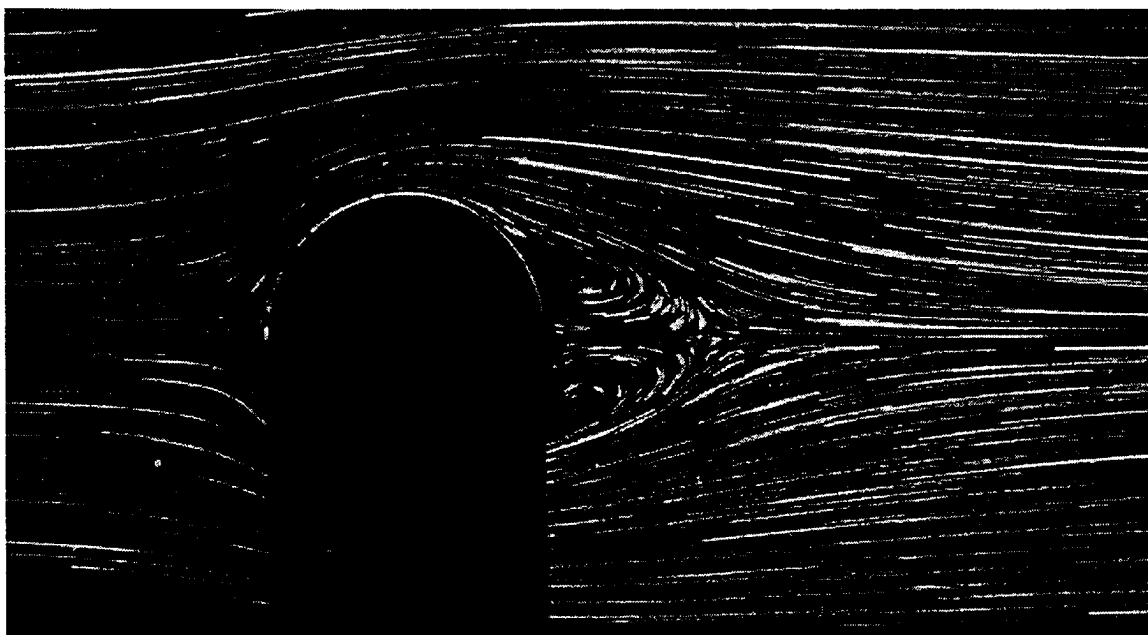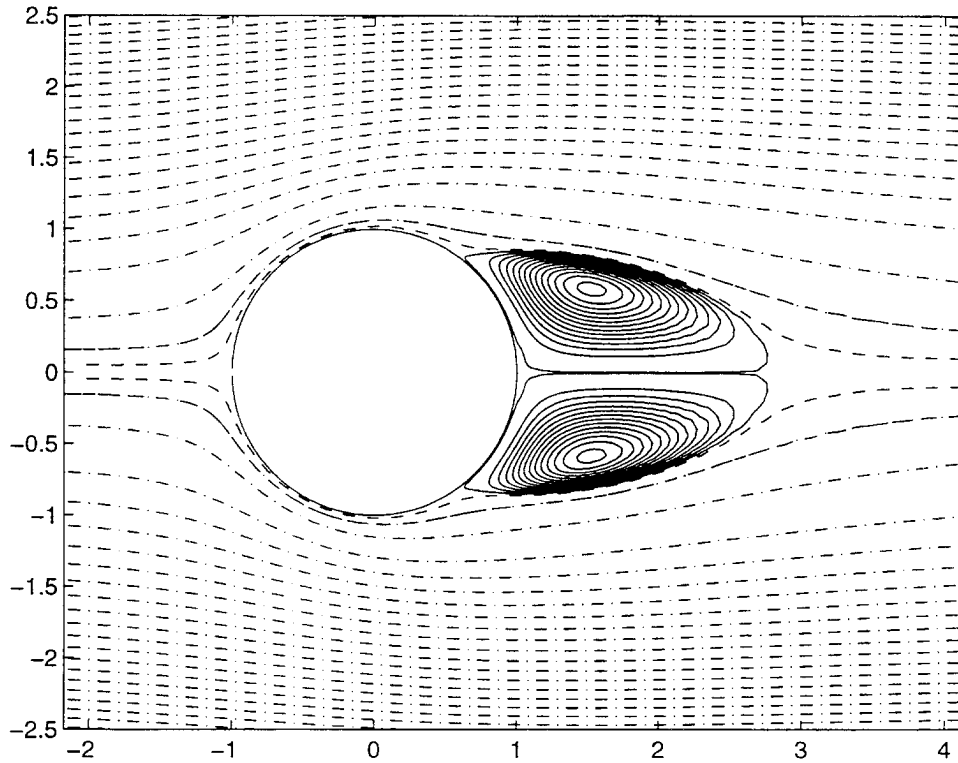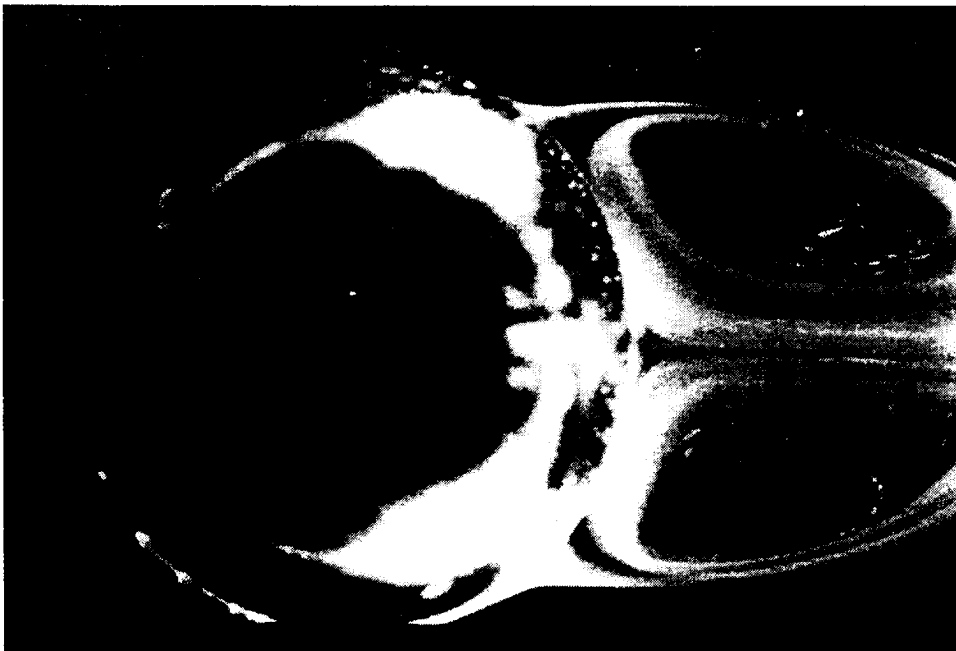

Figure 11. Visualization picture for Re = 104 by a thin coating of condensed milk on the sphere, which gradually melts and is carried into the stream of water. Taneda 1956.
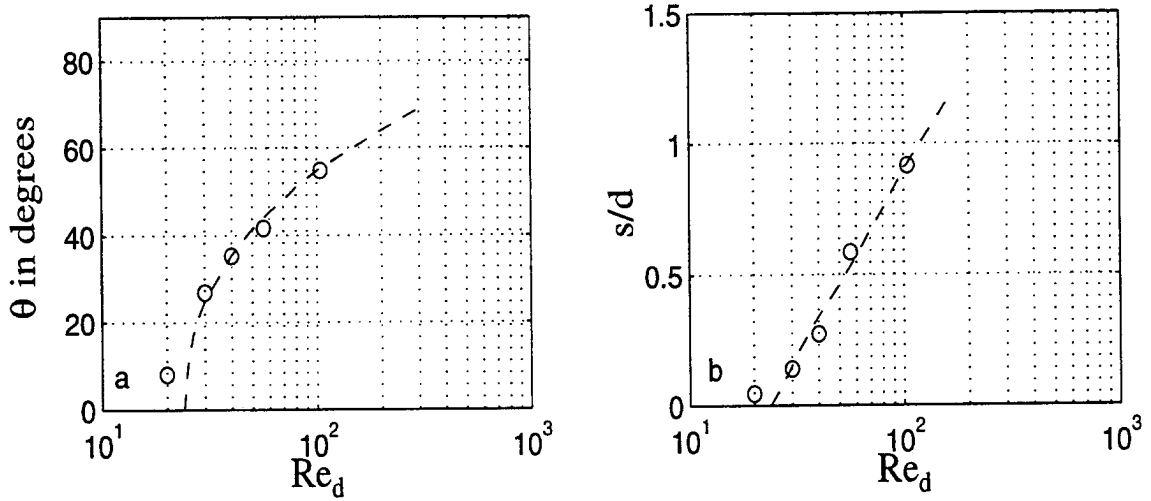
Figure 12.(a) Separation angle θ_s vs. Log Re (b) The ratio of bubble length to diameter (s/d) vs. Log Re '---' Taneda (1956)

C. BOUNDARY LAYER BEHAVIOR

Once the stream function was known for the particular flow the velocity over the sphere can be calculated by using the Eq.(3.7). The velocity in θ direction u_θ which is parallel to the surface of the sphere can be calculated by using the relation

$$u_\theta = -\frac{1}{r \sin\theta} \frac{\partial \psi}{\partial r} \qquad (5.11)$$

We also know from potential flow theory that the stream function is given by

$$\psi = \frac{1}{2}\left(r^2 - \frac{1}{r}\right)\sin^2\theta \qquad (5.12)$$

By using the relation in Eq.(5.11) u_θ can be calculated from Eq.(5.12) for potential flow as

$$u_\theta = \left(\frac{2r^3 + 1}{2r^3}\right)\sin\theta \qquad (5.13)$$

Figure 13 shows the $u_\theta/\sin\theta$ values which are obtained from Eq.(5.13) for potential flow along with the numerical results for various Reynolds numbers from this study. It is clearly observable that the velocity profile matches with the potential flow at

31

higher Reynolds numbers. The velocity profile for a small Reynolds number is also presented in Figure 13 for comparison, and shows that the velocity reaches its free stream value over a much larger distance in this Stokes flow regime.

Figure 13. The $u_\theta / \sin\theta$ profiles for varying Reynolds numbers ($\theta = \pi / 4$ from the nose) '-----' represents potential flow, solid lines represent numerical results.

The approach to boundary-layer behavior is now examined by comparing the boundary-layer thickness from numerical results with values of η_{peak} from boundary-layer analysis as discussed earlier in Chapter III.C. Figure 14 shows the η_{peak} values at corresponding Reynolds numbers along with the η_{peak} value as Re→∞ for a particular angle.

The η_{peak} values for corresponding Reynolds numbers can be modeled by assuming a model such as

$$\eta = C_1 + \frac{C_2}{Re^m} \tag{5.14}$$

where C_1 is the η_{peak} value as Re→∞, C_2 and m are the constants.

32

Figure 14. η_{peak} values vs. Log Re '---' represent the η_{peak} value as Re$\rightarrow\infty$

By using the η_{peak} values at Re=30, Re = 56.5 and Re = 104 , C_2 and m can be calculated from Eq.(5.14) as $C_2 = 2.464$ and m = 0.182 to obtain the model as

$$\eta = C_1 + \frac{2.464}{Re^{0.182}} \tag{5.15}$$

33

VI. CONCLUSIONS AND RECOMMENDATIONS

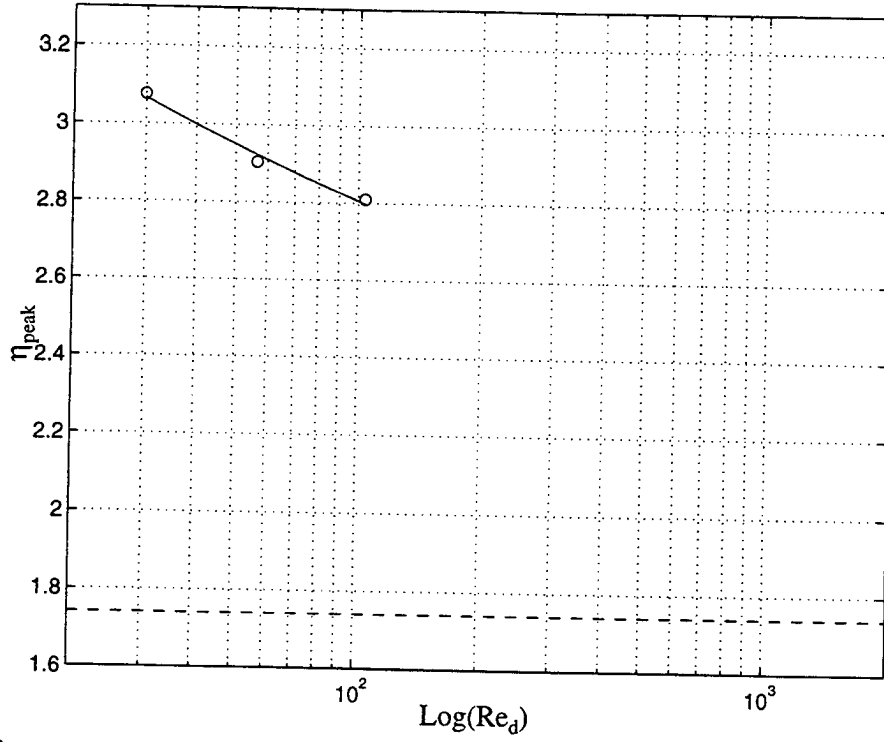The numerical results have showed a good agreement with the other results which were obtained by using different numerical methods. The pressure coefficient, C_p, which is one of two components of the total drag coefficient, C_d, couldn't be resolved for higher Reynolds numbers through the use of present method. But the calculated skin friction coefficients, C_f, and the stagnation-point pressure $k(\pi)$ have been resolved successfully.

A fine mapping for collocation points is very important to obtain more accurate results. The mapping parameters r_∞, α and L should be chosen in a way to provide enough collocation points in the boundary layer and recirculation regions. A finer mapping can increase the accuracy by allowing finer resolution in these large gradient regions.

The Green's function method that provides the natural development of vorticity along with the Neumann boundary conditions should not be considered as a trivial detail and must be used to have a stable convergence process.

A different FFT technique can be used which does not restrict the number of grid points to a power of two. This could reduce the memory requirement by allowing a relaxation in the choice of grid points.

Very good agreement has been obtained with the previous calculations and available experimental flow visualization pictures. This study is at a stage where it can now be extended to explore higher Reynolds numbers with suitable turbulent models.

APPENDIX A. PROGRAM STRUCTURE

In the first part of the program, problem parameters were defined such that Re, dt, L, r_inf, M, N. Calculations which don't depend on time were also performed in this part. In order to gain some additional memory D1, D2 and D3 matrices in (4.11)&(4.12) were calculated with the function D_Bmat and saved in terms of diagonal elements only. Non-diagonal elements of these matrices were included separately in each iteration.

Calculations showed that the matrix M1 (derivative operator in r direction) and consequently the matrix M3 and the block matrices which are formed by the diagonals of D1, D2 and D3 are ill-conditioned. To avoid the numerical errors in solving the systems of equations, Singular Value Decomposition (SVD) method was used. SVD of the matrices and calculations of w and c that are used in Green Function method were performed in this part. The built-in function SVD in MATLAB, was used for decompositions of the matrices in the systems of equations.

The calculation part basically consists of four steps. In first step, A_{ij} matrix was calculated from eqn. (4.22) out of the time loop. In second step, inside the time loop the particular solutions of w and c were found from eq. (4.17) and (4.18). In third step, H that is used in Green's Function method, was calculated and finally homogenous and particular solutions are combined to get w and c.

Most of the calculations were performed in *spectral domain*. Only nonlinear operations were done in *physical domain*. Nonlinear terms were calculated with the functions nonlin for w-c equations .

A convergence criterion isn't used in the program to avoid the wrong results which are caused by the over-shooting for high Reynolds numbers. Instead, the results are checked during the calculations and program was terminated after seeing the steady state.

Solsvd : This function is used to solve equations after SVD in Matlab. A limit, which is defined as a number smaller than the values of S matrix in SVD, is used in this function to avoid the numerical errors due to those ill-conditioned matrices. This is

avoided by forcing those singular values which are smaller than the defined limit, to zero. 10^{-14} is used in all calculations.

Solsvd1 : Since this function was used for solving homogenous parts in Green's Function method and performed once before the time-loop, no limit was used in *solsvd1*.

Phy : This function was used for transformations of the variables from *spectral domain* to *physical domain*

Operat : Derivatives in θ direction in *spectral domain* was performed with the function, *operat*. Since these terms were used only in nonlinear terms the output from this function is in *physical domain*.

L : Mapping parameter

Re : *Reynold's* Number

dt : Time interval between iterations

r_inf : Outer boundary

step : Number of iterations

N : Number of grid points in θ direction.

M : Number of grid points in r direction.

xcor, ycor : Cartesian coordinates of grid points with respect to center of sphere. (used for presentation of the results)

M1 : Derivative operator in r direction.

D1, D2, D3 : Matrixes defined as in (4.11)&(4.12)

ω : Vorticity.

c : Potential function as in (3.15a)&(3.26)

wtil, ctil : Homogenous part of the ω and c defined as in Green Function.

Aij, H, landa : Variables defined as in Green's function method in chapter IV.

wp, cp : Particular solution of ω and c defined as in Green Function.

Cf : The frictional component of drag

kpi : Non-dimensional pressure coefficient at $\theta = \pi$

Cp : Pressure component of drag

APPENDIX B. PROGRAM CODES

```
%% define program parameters
% Table 1 list these parameters for every Reynolds numbers
clear all
global E M1 M2 M3
L=8;Re=1;dt=0.02;
r_inf=250;step=10000;

%% define grid points

N=32;n=[0:N-1]';
teta=n.*pi./N;
M=32;m=[0:M]';
z=cos(pi.*m./M);
b=1+2*L/(r_inf-1); % map=1
r=1+L.*(1+z)./(b-z);% map=1
global N M
xcor=cos(teta)*r';
ycor=sin(teta)*r';

E=emat(M);
disp('E matrix is done')

%%  define M1,M2,M3

dz_dr=(b.*(L+r-1)-b.*(r-1)+L)./(L+r-1).^2; % map=1
B=diag(dz_dr);
M1=B*E;
R=diag(r);global R Re dt
M2=R*M1;
M3=R*(2.*eye(M+1)+M2)*M1;

%% define D1 D2 D3

[D1,D2,D3]=D_Bmat(M,N);

%  define initial w c wp cp u

dum1=(-1.5./r.^2)*sin(teta'))';
dum2=[dum1;zeros(1,M+1);-1.* flipud(dum1(2:N,:))];
dum3=fft(dum2);
```

```
w=imag(dum3(1:N, :))];w=w';
dum1=(-0.75+0.25./r.^2)*sin(teta'))';
dum2=[dum1;zeros(1,M+1);-1.*flipud(dum1(2:N,:))];
dum3=fft(dum2);c=imag(dum3(1:N,: ))];c=c';
wp=zeros(M+1,N);cp=wp;

%  define kmat (for teta der.) and cotteta (for nonlinear terms)

dum=ones(1,M+1);
kmat=n*dum;
cotteta=[0;cot(teta(2:N))]*dum;
global kmat cotteta teta

%  svd decomposition for D1 D3 and define rsquare (nonlinear)

D1u=zeros(N*(M+1),M+1);
D1l=D1u;D1p=D1u;D3l=D1u;D3u=D1u;D3p=D1u;
rsquare=zeros(M+1,N);
for i=1:N
  bas=(i-1)*(M+1)+1;
  son=bas+M;
  rsquare(:,i)=r.^2;
  D1(bas,:)=[1 zeros(1,M)]; % modify D1 for w @ r=inf
  D1(son,:)=[zeros(1,M) 1]; % modify D1 for w @ r=1
  [D1l(bas:son,:),D1u(bas:son,:),D1p(bas:son,:)]=svd(D1(bas:son,:));
  D3(bas,:)=[1 zeros(1,M)]; % modify D3 for c @ r=inf
  D3(son,:)=[zeros(1,M) 1]; % modify D3 for c @ r=1
  [D3l(bas:son,:),D3u(bas:son,:),D3p(bas:son,:)]=svd(D3(bas:son,:));
end
global rsquare

%  define c_ c_teta c_r u_ u_teta u_r

c_=(0.5.*sin(teta))*r';
c_teta=0.5.*cos(teta))*r';
c_r=-(0.5*sin(teta))*ones(1,M+1);
global c_ c_teta c_r

%  define c boundary at r=1

dum4=-0.5.*sin(teta);
dum5=[dum4;0;-1.* flipud(dum4(2:N,:))];
dum6=fft(dum5);
cbr1=imag(dum6(1,N))';
```

40

```
% begin green function wtil ctil

wtil=zeros(M+1,N^2);
ctil=wtil;

for jj=1:N
  RR=zeros(M+1,N);
  dum1=[zeros(1,jj-1) 1 zeros(1,N-jj)];
  dum2=[dum1 0 -1.*fliplr(dum1(2:N))];
  dum3=fft(dum2);
  dum4=imag(dum3(1:N));if jj==1;dum4=real(dum3(1:N));end;
  RR(M+1,:)=dum4;
  wtil(:,jj*N)=solsvd1(D1l((N-1)*(M+1)+1:(N-1)*(M+1)+1+M,:),...
          D1u((N-1)*(M+1)+1:(N-1)*(M+1)+1+M,:),...
          D1p((N-1)*(M+1)+1:(N-1)*(M+1)+1+M,:),...
          RR(:,N));

  for i=N-1:-1:1
    sum=zeros(M+1,1);
    ii=(jj-1)*N+i;
    for j=i+1:N
        if rem(i+j,2)==2
            sum=sum+(-2*(i-1)).*wtil(:,(jj-1)*N+j);
        end
    sum(1)=0;
    sum(M+1)=0;
    end
    RR_=RR(:,i)-sum;

    wtil(:,ii)=solsvd1(D1l((i-1)*(M+1)+1:(i-1)*(M+1)+1+M,:),...
            D1u((i-1)*(M+1)+1:(i-1)*(M+1)+1+M,:),...
            D1p((i-1)*(M+1)+1:(i-1)*(M+1)+1+M,:),...
            RR_);

  end

  tempwtil=(-1.*rsquare).*wtil(:,(jj-1)*N+1:jj*N);
  tempwtil(M+1,:)=zeros(1,N);
  tempwtil(1,:)=zeros(1,N);
  ctil(:,jj*N)=solsvd1(D3l((N-1)*(M+1)+1:(N-1)*(M+1)+1+M,:),...
          D3u((N-1)*(M+1)+1:(N-1)*(M+1)+1+M,:),...
          D3p((N-1)*(M+1)+1:(N-1)*(M+1)+1+M,:),...
          tempwtil(:,N));
```

41

```
for i=N-1:-1:1
    ii=(jj-1)*N+i;
    sum=zeros(M+1,1);
    for j=i+1:N
        if rem(i+j,2)==2
            sum=sum+(-2*(i-1)).*ctil(:,(jj-1)*N+j);
        end
        sum(1)=0;
        sum(M+1)=0;
    end
    wtil_=tempwtil(:,i)-sum;

    ctil(:,ii)=solsvd1(D3l((i-1)*(M+1)+1:(i-1)*(M+1)+1+M,:),...
            D3u((i-1)*(M+1)+1:(i-1)*(M+1)+1+M,:),...
            D3p((i-1)*(M+1)+1:(i-1)*(M+1)+1+M,:),...
            wtil_);
  end
end

% find Aij matrix

for jj=1:N
    blok=ctil(:,(jj-1)*N+1:jj*N);
    dum1=phy(blok')';
    dum2=(M1*dum1)';
    dum3=[dum2; zeros(1,M+1) ; -1.*flipud(dum2(2:N,:))];
    dum4=fft(dum3);dum5=imag(dum4(1:N,:));dum5=dum5';
    ctilr_1(jj,1:N)=dum5(M+1,:);
end

Aij=ctilr_1';

% find svd of Aij for landa solving

Aij(1,:)=[1 zeros(1,N-1)];
[Aiju,Aijs,Aijv]=svd(Aij);

% begin time loop

for ops=1:step

    if ops==1;prc=c;prw=w;pru=u;end
```

42

```
% find R1

R1=zeros(M+1,N);
R1(:,N)=D2((N-1)*(M+1)+1:(N-1)*(M+1)+1+M,:)*w(:,N);
for i=N-1:-1:1
   summ=zeros(M+1,1);
   for j=i+1:N
       if rem(i+j,2)==2
          summ=summ+(-2*(i-1)).*w(:,j);
       end
   end
   R1(:,i)=D2((i-1)*(M+1)+1:(i-1)*(M+1)+1+M,:)*w(:,i)+summ;
end
R1=-1.*R1;

%  find R2

R2a=nonlin(w,c);
R2b=nonlin(prw,prc);
R2=3/2.*R2a-1/2.*R2b;
R2=(-1*Re).*rsquare.*R2;
Rtot=R1+R2;
prw=w;prc=c;

%% green function solution

% find new wp

%% apply BC for wp

Rtot(1,:)=zeros(1,N);   % BC for wp=0 at r_inf
Rtot(M+1,:)=zeros(1,N);  % BC for wp=0 at r_1

wp(:,N)=solsvd(D1l((N-1)*(M+1)+1:(N-1)*(M+1)+1+M,:),...
        D1u((N-1)*(M+1)+1:(N-1)*(M+1)+1+M,:),...
        D1p((N-1)*(M+1)+1:(N-1)*(M+1)+1+M,:),...
        Rtot(:,N));

for i=N-1:-1:1
   sum=zeros(M+1,1);
   for j=i+1:N
       if rem(i+j,2)==2
          sum=sum+(-2*(i-1)).*wp(:,j);
       end
```

```
      sum(1)=0;
      sum(M+1)=0;
    end
    Rtot_=Rtot(:,i)-sum;

    wp(:,i)=solsvd(D1l((i-1)*(M+1)+1:(i-1)*(M+1)+1+M,:),...
            D1u((i-1)*(M+1)+1:(i-1)*(M+1)+1+M,:),...
            D1p((i-1)*(M+1)+1:(i-1)*(M+1)+1+M,:),...
            Rtot_);

end

%  solve for new cp

tempwp=-1.*rsquare.*wp;
tempwp(M+1,:)=cbr1; % BC for cp=-c_r at r_1 zero for pure spin
tempwp(1,:)=zeros(1,N); % BC for cp=0 at r_inf

cp(:,N)=solsvd(D3l((N-1)*(M+1)+1:(N-1)*(M+1)+1+M,:),...
        D3u((N-1)*(M+1)+1:(N-1)*(M+1)+1+M,:),...
        D3p((N-1)*(M+1)+1:(N-1)*(M+1)+1+M,:),...
        tempwp(:,N));

for i=N-1:-1:1
    sum=zeros(M+1,1);
    for j=i+1:N
        if rem(i+j,2)==2
            sum=sum+(-2*(i-1)).*cp(:,j);
        end
    sum(1)=0;
    sum(M+1)=0;
    end
    w_=tempwp(:,i)-sum;

    cp(:,i)=solsvd(D3l((i-1)*(M+1)+1:(i-1)*(M+1)+1+M,:),...
            D3u((i-1)*(M+1)+1:(i-1)*(M+1)+1+M,:),...
            D3p((i-1)*(M+1)+1:(i-1)*(M+1)+1+M,:),...
            w_);
end

% find landa
% find H

dum1=phy(cp')';
```

```
dum2=(M1*dum1)'; % NxM+1
dum3=-1.*c_r-dum2;
dum4=[dum3;zeros(1,M+1);-1.*flipud(dum3(2:N,:))];
dum5=fft(dum4);
dum6=imag(dum5(1:N,:));
dum6=dum6'; % M+1xN

H=dum6(M+1,:);H=H'; % Nx1
H(1)=0;
landa=solsvd(Aiju,Aijs,Aijv,H);

% find complete w & c

dum1c=zeros(M+1,N);dum1w=dum1c;
for jj=1:N
  blokc=ctil(:,(jj-1)*N+1:jj*N);
  blokw=wtil(:,(jj-1)*N+1:jj*N);
  dum2c=landa(jj).*blokc;
  dum2w=landa(jj).*blokw;
  dum1c=dum1c+dum2c;
  dum1w=dum1w+dum2w;
end

w=wp+dum1w;
c=cp+dum1c;

res=phy(w');
resp=phy(prw');
resc=phy(c');
resc=resc+c_;

% Calculate Cf for every iteration
  dum1=res(:,M+1);
  dum2=(sin(teta)).^2;
  dum3=dum1.*dum2;
  cf(ops)=-4/Re*trapz(teta,dum3);

% Calculate k(π) for every iteration

dum1=w';
for i=1:M+1
    sum(i)=0;
    for j=1:N
        f=((j-1)*dum1(i,j).*(-1.^(j-1)))./N;
```

```
         sum(i)=sum(i)+f;
     end
   end
   dum2=(1./r).*sum;
   kpi(ops)=(1+(8/Re)*trapz(r,dum2));

% Check for convergence

   if max(max(isnan(w)))==1;error(' it blowed up!!!! ');end
% Save the variables to a file
save tez.mat c w Re ops r_inf cf kpi L N M dt;
end  % end of time loop
%%%%%

function [D1,D2,D3]=D_Bmat(M,N)
global M3 R dt Re
k=(M+1)*N;
D1=zeros(k,M+1);
D2=zeros(k,M+1);
D3=zeros(k,M+1);
for i=1:N
  for j=i:N
   if i==j
      D1((i-1)*(M+1)+1:(i-1)*(M+1)+1+M,:)...
=M3+(-1*(i-1)*(i).*eye(M+1)-Re/dt.*R.^2);
      D2((i-1)*(M+1)+1:(i-1)*(M+1)+1+M,:)...
=M3+(-1*(i-1)*(i).*eye(M+1)+Re/dt.*R.^2);
      D3((i-1)*(M+1)+1:(i-1)*(M+1)+1+M,:)...
=M3+(-1*(i-1)*(i).*eye(M+1));
   end
  end
end
%%%%%%
function E=emat(M)
E=zeros(M,M);
m=0:M;
z=cos(pi.*m./M);
for i=0:M
   for j=0:M
     if i~=j
       if ((i==0 | i==M) &  (j==0 | j==M)) | ((i~=0 & i~=M) &  (j~=0 & j~=M))
         c=1;else
       if (i==0 | i==M) &  (j~=0 & j~=M)
         c=2;else
```

46

```
          if (i~=0 & i~=M) &  (j==0 | j==M)
            c=1/2;end;end;end;
            E(i+1,j+1)=c*(-1)^(i+j)/(z(i+1)-z(j+1));
        else;
          if i==0
            E(i+1,j+1)=(2*M^2+1)/6;
          else
            if i==M
              E(i+1,j+1)=(2*M^2+1)/(-6);
            else
              E(i+1,j+1)=-1*z(j+1)/(2*(1-z(j+1)^2));
            end
          end
        end
      end
end
%%%%%%%

function R2=nonlin(w,c)
global kmat rsquare cotteta N M M1 c_ c_teta c_r teta
%  variable list
%
%  dw/dteta=non1 dc/dteta=non2 dw/dr=non3 dc/dr=non4 (in phy)
%
%  transpose matrices for column operations in teta direction
r=sqrt(rsquare)';
w=w';c=c';
non1=operat(w);
non2=operat(c);
wph=phy(w);cph=phy(c);
non3=[M1*wph'];
non4=[M1*cph']';non4(:,M+1)=-0.5.*sin(teta);

term1=-1./r.*non3.*(non2+c_teta);
term2=1./r.*non1.*(non4+c_r);
term3=-1.*cotteta./r.*wph.*(non4+c_r);
term4=-1.*cotteta./r.*non3.*(c_+cph);
term5=wph./rsquare'.*(non2+c_teta);
term6=(c_+cph)./rsquare'.*non1;
term0=term1+term2+term3+term4+term5+term6;

ter=[term0;zeros(1,M+1);-1.*flipud(term0(2:N,:))];
RR2=fft(ter);
R2=imag(RR2(1:N,:));R2=R2';
```

```
%%%%%%%

function y=operat(x)
global N M kmat
re=zeros(N,M+1);
X=re+i.*x;
Y=i.*kmat.*X;
Y_ful=[Y;zeros(1,M+1);flipud(Y(2:N,:))];
y=ifft(Y_ful);
y=real(y(1:N,:));

%%%%%%%
function y=phy(x)
global N M
re=zeros(size(x));
X=re+i.*x;
Y_ful=[X;zeros(1,M+1);conj(flipud(X(2:N,:)))];
dum=ifft(Y_ful);
y=real(dum(1:N,:));

%%%%%%

function y=solsvd1(u,s,v,b)
w=diag(s);
wmin=max(w)*1e-12;
for i=1:length(w)
  if w(i)<wmin;ww(i)=0;else;ww(i)=1/w(i);end
end
www=diag(ww);
y=v*www*(u'*b);

%%%%%%

function y=solsvd(u,s,v,b)
w=diag(s);
%wmin=max(w)*1e-8;
for i=1:length(w)
%  if w(i)<wmin;ww(i)=0;else;ww(i)=1/w(i);end
  ww(i)=1/w(i);
end
www=diag(ww);
y=v*www*(u'*b);
```

LIST OF REFERENCES

Auton, T.R., Hunt, J.C.R. and Prudhome, M.,1988, *"The force exerted on a body in inviscid steady non-uniform rotational flow,* Journal of Fluids Mechanics, Vol.197, pp241-257

Bassett, A.B.,1888, *A Treatise in Hydrodynamics,Vol.II,* Deighton, Bell, an Co.

Batchelor, G.K,1967, *An Introduction to Fluid Dynamics,* Cambridge University Press.

Bentwich, M. & Miloh, T.,1978, *"The unsteady matched Stokes-Oseen solution for the flow past a sphere,* Journal of Fluids Mechanics, Vol.88, pp17-32

Brabston, D.C. & Keller, H.B.,1975, *"Viscous flows past spherical gas Bubbles",* Journal of Fluids Mechanics, Vol.69, Part.I, pp179-189

Canuto, C., Hussaini, M.Y., Quarteroni, A. and Zang, T.A.,1988, *Spectral Methods in Fluid Dynamics,* New York : Springer-Verlag

Chang, E.J,1992, *Accelerated motion of rigid spheres in unsteady flow at low to moderate numbers,* PhD thesis, Brown University

Chang, E.J. and Maxey, M.R.,1994, *"Unsteady flow about a sphere at low to moderate Reynolds number. Part I. Oscillatory motion",* Journal of Fluids Mechanics, Vol.277, pp347-349

Chester, W. & Breach, D.R.,1969, *"On the flow past a sphere at low Reynolds number",* Journal of Fluids Mechanics, Vol.37, pp.751-760

Dennis, S.C.R. & Walker, J.D.A,1971, *"Calculation of the steady flow past a sphere at low and moderate Reynolds numbers",* Journal of Fluids Mechanics, Vol.48, pp.771-789

Dennis, S.C.R. & Walker, J.D.A,1972, *"Numerical solutions for time-dependent flow past an impulsively started sphere",* Phys. Fluids, Vol.15, pp.517-525

Fornberg, B.,1988, *"Steady viscous flow past a sphere at high Reynolds numbers",* Journal of Fluids Mechanics, Vol.190, pp.471-489

Goldstein, S.,1929, *"The forces on a solid body moving through viscous fluid",* Proc.R.Soc.London, A.123, pp.216-235

Gottlieb, D. and Orszag, S.A.,1977, *Numerical Analysis of Spectral Methods: Theory and Applications.*, Philadelphia: SIAM

Homann, F.,1936, *"The effect of high viscosity on the flow around a cylinder and around a sphere"*, NACA.Tech.Mem.1334.

Kim, I. & Pearlstein, A.J.,1990, *"Stability of flow past a sphere"*, Journal of Fluids Mechanics, Vol.211, pp.73-93

Le Clair, B.P., Hamielec, A.E. & Pruppracher, H.R.,1970, *"A numerical study of the drag on a sphere at low and intermediate Reynolds numbers"*, J.Atmos.Sci.Vol.27, pp.308-315

Lin, C.L. & Lee, S.C.,1973, *"Transient state analysis of separated flow around a sphere"*, Compu. Fluids, Vol.1, pp.235-250

Marcus, P.S. and Tuckerman,L.S.,1987, *"Simulation of flow between concentric rotating spheres. Part I. Steady states."*, Journal of Fluids Mechanics, Vol.185, pp1-30

Maxey, M.R. & Riley, J.J.,1983, *"Equation of motion for a small rigid sphere in a nonuniform flow"*, Phys.Fluids.Vol26, pp.863-889

Odar, F.,1964, *"Forces on a sphere accelerating in a viscous fluid"*, US Army Cold Regions Research and Engineering Laboratory, Research Rep.128

Odar, F. & Hamilton, W.S.,1963, *"Forces on a sphere accelerating in a viscous fluid"*, Journal of Fluids Mechanics, Vol.18, pp.302-314

Oliver, D.L.R. & Chung, J.N.,1985, *"Flow about a fluid sphere at low to moderate Reynolds numbers"*, Journal of Fluids Mechanics, Vol.177, pp.1-18

Orszag, S.A.,1974, *"Fourier series on spheres"*, Mon.Weath.Rev., Vol.102, pp.56-75

Panton, R.L.,1996, *Incompressible Flow: Second Edition, Appendix D*, New York: John Wiley & Sons Inc.

Rimon, Y. & Cheng, S.I.,1969, *"Numerical solution of a uniform flow over a sphere at intermediate Reynolds numbers"*, Phys. Fluids , Vol.12, pp.949-959

Rosenhead, L.,1963, *Laminar Boundary Layers, pp.417-426*, Dover Publications, Inc., New York.

Sano, T.,1981, *"Unsteady flow past a sphere at low Reynolds number"*, Journal of Fluids Mechanics, Vol.112, pp.433-441

Schlichting, H.,1987, *Boundary-Layer Theory, pp.235-239,* McGraw-Hill, Inc.

Taneda, S.,1956, *"Experimental investigation of the wake behind a sphere at low Reynolds numbers",* J.Phys.Soc., Japan 11, pp.302

Van Dyke, M.,1982, *An Album of Fluid Motion,* The Parabolic Press, Stanford, Ca.

INITIAL DISTRIBUTION LIST

No. Copies

1. Defense Technical Information Center... 2
   8725 John J. Kingman Rd., STE 0944
   Ft. Belvoir, VA 22060-6218

2. Dudley Knox Library 2
   Naval Postgraduate School
   411 Dyer Rd.
   Monterey, CA 93943-5101

3. Chairman, Code ME 1
   Department of Mechanical Engineering
   Naval Postgraduate School
   Monterey, CA 93943-5000

4. Professor Ashok Gopinath, Code ME/GK 2
   Department of Mechanical Engineering
   Naval Postgraduate School
   Monterey, CA 93943-5000

5. Naval Engineering Curricular Office, Code 34 1
   Naval Postgraduate School
   Monterey, CA 93943-5000

6. Deniz Kuvvetleri Komutanligi 1
   Personel Daire Baskanligi
   Bakanliklar, Ankara, Turkey 06100

7. Deniz Harp Okulu Komutanligi 1
   Tuzla, Istanbul, Turkey 81704

8. Zekai AKCAN 3
   Afyon Cad. Oren Apt. No.3/13
   Kutahya , Turkey 43020

9. I. T. Ü. Makina Müh. Bl. 1
   Ratip Berker Kütüphanesi
   Maslak, Istanbul, Turkey